

Deformation dependent permeability from variationally consistent homogenization

Downloaded from: https://research.chalmers.se, 2025-11-09 13:41 UTC

Citation for the original published paper (version of record):

Rollin, D., Larsson, F., Runesson, K. et al (2025). Deformation dependent permeability from variationally consistent homogenization. GAMM Mitteilungen, 48(4). http://dx.doi.org/10.1002/gamm.70010

N.B. When citing this work, cite the original published paper.

research.chalmers.se offers the possibility of retrieving research publications produced at Chalmers University of Technology. It covers all kind of research output: articles, dissertations, conference papers, reports etc. since 2004. research.chalmers.se is administrated and maintained by Chalmers Library

ORIGINAL ARTICLE



Check for updates

Deformation dependent permeability from variationally consistent homogenization

David René Rollin¹ | Fredrik Larsson² | Kenneth Runesson² | Ralf Jänicke¹

²Department of Industrial and Materials Science, Chalmers University of Technology, Gothenburg, Sweden

Correspondence

David René Rollin, Institute of Applied Mechanics, Technische Universität Braunschweig, Braunschweig, Germany. Email: d.rollin@tu-braunschweig.de

Funding information

Vetenskapsrådet, Grant/Award Numbers: 2020-05057, 2024-05854

Abstract

In this article, the influence of large deformations on the effective permeability of a bicontinuous porous material is investigated. On the fine-scale, Neo-Hooke hyperelasticity is considered for the solid skeleton. In a third medium approach, we model the pore space as filled with a softer material of the same type. Fluid flow through the deformed pores is expressed in terms of a Stokes' flow model. The influence of the pore pressure on the deformation is neglected, resulting in a one-way coupling which allows for a sequential solution of the two physical problems. The framework of Variationally Consistent Homogenization is used to derive a two-scale formulation based on a Representative Volume Element (RVE) characterizing the microstructure. Finally, a two-step procedure to compute the deformation dependent permeability is established: Firstly, the deformation of the RVE for a given macroscale deformation gradient is computed. Secondly, sensitivities for the fluid flow through the deformed RVE are computed and used to determine the effective permeability tensor. A numerical study is conducted for sets of RVEs with the same material parameters and different porosity. For the case of uniaxial compression, a significant influence of the deformation on the effective permeability is observed: For a macroscale compression of 20%, the effective permeability orthogonal to the compression direction is reduced by almost 60%.

KEYWORDS

effective permeability, large deformations, variationally consistent homogenization

1 | INTRODUCTION

In a variety of fields and applications, the prediction of fluid flow through a porous medium is of interest. Some examples are geologic formations [24], concrete structures [11], and proton exchange membrane electrolyzers [23]. In most cases, resolving the porous material numerically would result in excessive computational cost. It is, therefore, preferable to employ a phenomenological model or use computational homogenization to 'derive' the macroscale response. For low Reynold's numbers, it is common to adopt Darcy's law which relates the seepage velocity to the macroscale pressure gradient via the effective permeability of the porous medium [2, 21]. To determine the effective permeability can, indeed, turn

This is an open access article under the terms of the Creative Commons Attribution License, which permits use, distribution and reproduction in any medium, provided the original work is properly cited.

© 2025 The Authors. $G\!AMM$ - Mitteilungen published by Wiley-VCH GmbH.

¹Institute of Applied Mechanics, Technische Universität Braunschweig, Braunschweig, Germany

out as a challenging task both experimentally and numerically. Over the years, a great number of methods for estimating the effective permeability have been presented (see [4, 14, 16, 17] for reviews).

Depending on the application in mind, the interaction of the fluid flow with other physical fields are of interest: First and foremost, the fluid flow in the pore space interacts with the deformation of the surrounding matrix [20]. Further, the flows of multiple fluids may interact [1, 24]. Other effects might cause a transported species to be bound physically or chemically to the matrix material [11].

Within the field of computational homogenization, different techniques have already been applied to this type of problem. For example, asymptotic expansion based on Stokes flow coupled to linear elastic deformation has been presented in [15]. Variationally Consistent Homogenization (VCH) has been applied to a nonlinear flow problem in [18]; however, not accounting for interactions with the solid matrix.

In this contribution, we consider the deformation dependent permeability in a finite strain setting. First, the deformation of a porous medium is described for large deformations using a compressible Neo–Hookean material model. In this step, the pore space is considered to be a soft solid to avoid self-penetration of the surrounding matrix. Next, a model of Stokes flow in the deformed pore space is considered. A pull-back operation with the deformation gradient from the first step is applied to express the problem in the undeformed configuration. The framework of VCH is applied to derive the macroscale problem and an upscaling procedure from a Representative Volume Element (RVE).

The two key points of the one-way coupling are:

- (i) We consider different time scales for the mechanical deformation (slow) and the Stokes flow problem (fast). As a consequence, the flow state during deformation can be assumed to be always close to equilibrium.
- (ii) The pore pressure magnitude is assumed to be small compared to the stresses related to the deformation.

Therefore, the action of fluid pressure on the solid skeleton is disregarded.

This approach allows for a sequential computation of the two physical problems. In reality, such a sequential order of the process occurs, for example, during the production of components made of a soft porous material, such as the assembly of electrolysis cells. In this case, the production process involves large deformation and one is interested in the influence of the deformation on the permeability of the final product. For this type of application, we develop a consistent homogenization method based on sets of RVEs with a realistic three-dimensional, bi-continuous microstructure. A third medium approach is used to account for large deformations of the pore system. Moreover, direct upscaling is used to efficiently compute the deformation dependent effective permeability.

The article is organized as follows: First, the balance and constitutive equations for the mechanical and fluid flow problem on the fine-scale are presented in Section 2. Next, based on the concept of VCH, the pertinent two-scale analysis is established in Section 3. The RVE-problem and the consequent upscaling procedure are considered in Section 4. Computational results are presented and compared in Section 5. Finally, concluding remarks and an outlook to future work are given in Section 6.

Regarding notation, meager type is used to denote scalars, whereas bold type is used to denote vectors as well as higher order tensors. Scalar product (single contraction) is denoted by a dot. For example, for two vectors $\boldsymbol{a}, \boldsymbol{b}$ and a second order tensor \boldsymbol{A} , we have $\boldsymbol{a} \cdot \boldsymbol{b} = a_i b_i$ and $(\boldsymbol{A} \cdot \boldsymbol{b})_i = (\boldsymbol{A})_{ij}(\boldsymbol{b})_j$ in terms of their Cartesian components, where the Einstein summation convention is used. To be consistent with index notation, $\diamondsuit \cdot \nabla$ (and not $\nabla \cdot \diamondsuit$) denotes the divergence (i.e. $(\diamondsuit)_{ij,j}$).

2 | FINE-SCALE MODEL

2.1 | Preliminaries

We consider a domain Ω with a fully resolved bicontinuous microstructure comprising a solid skeleton Ω^S with a pore system Ω^P which is saturated with a fluid. The external boundary is denoted Γ and the interface of the phases is denoted $\Gamma^i = \partial \Omega^S \cap \partial \Omega^P$. On Γ we define N as the outward pointing normal vector in the initial configuration, while on Γ^i we define N as the normal vector pointing into Ω^S . Accounting for finite deformations, the corresponding quantities in the current configuration are denoted ω , ω^S , ω^P , γ , γ^i , and n.

We consider a one-way coupled setting of mechanical deformation and flow of the incompressible fluid in the pore space. Firstly, we assume that the contribution of the fluid to the mechanical response is negligible. Thus, for the

.com/doi/10.1002/gamm.70010 by Chalmers University Of Technology, Wiley Online Library on [07/11/2025]. See the Terms

mechanical problem, the pore space can be considered drained and the deformation can be computed independently of the fluid pressure. After the deformation of the fluid domain has been computed, the flow of the fluid inside the deformed pore space is computed in a separate step.

2.2 | Mechanical problem

The deformation of the system is described by the mapping

$$\varphi = \begin{cases} \varphi^{S} : \Omega^{S} \to \omega^{S} \\ \varphi^{P} : \Omega^{P} \to \omega^{P} \end{cases}$$
(1)

with $\varphi(X) = X + u(X)$ where u(X) is the displacement field in a point $X \in \Omega$. The deformation gradient is denoted $F = \varphi \otimes \nabla_X = I + u \otimes \nabla_X$, where I is the second order identity tensor and ∇_X denotes the nabla operator in the reference configuration, and $J = \det F$ is the Jacobian.

We consider the case of a drained (stress-free) pore space. In order to

- (i) establish the complete map φ and
- (ii) to prevent penetration of solid constituents

we shall consider a soft, yet aversive (enforcing J > 0) elasticity model in the pore space. This type of model for an empty space is often referred to as third medium approach [9, 22].

With σ as the Cauchy stress and $P := J\sigma \cdot F^{-T}$ as first Piola-Kirchhoff stress tensor, we adopt the material models

$$P(F) = \begin{cases} P^{S}(F) & \text{in } \Omega^{S} \\ P^{P}(F) & \text{in } \Omega^{P} \end{cases}$$
 (2)

We choose a Neo-Hooke hyperelastic model for the stress in both phases. With the right Cauchy-Green deformation tensor $C = F^T \cdot F$, the constitutive relation becomes

$$P(F) = F \cdot \left[G[I - C^{-1}] + \lambda \ln(J)C^{-1} \right], \tag{3}$$

where λ and G are the Lamé parameters. Before contact, the influence of the material in the pore space should be negligible. Thus, a very low stiffness in this phase is desirable. However, close to contact, the stress dramatically increases due to the logarithmic term in (3), which impedes solving the problem. A larger stiffness of the pore space can reduce the deformation of this phase and by that to some extend avoid the extreme region of the logarithmic expression. Yet, this would imply a less accurate description of the problem before contact. Alternatively, regularization can be used to make the low stiffness at contact computationally feasible (cf. [9, 22]). Here, regularization will not be discussed, because the focus is on how to obtain the effective permeability for a deformed pore space.

To apply boundary conditions, the external boundary is split as $\Gamma = \Gamma_D^u \cup \Gamma_N^u$ into a Dirichlet part Γ_D^u and a Neumann part Γ_N^u . On Γ_D^u the displacement \boldsymbol{u}^{pre} and on Γ_N^u the traction \boldsymbol{T}^{pre} is prescribed. With this, the strong form of the mechanical problem reads: Find $\boldsymbol{u}:\Omega\to\mathbb{R}^3$ that solves

$$-\mathbf{P}\cdot\mathbf{\nabla}_{X}=0\qquad\text{in }\Omega,\tag{4a}$$

$$\boldsymbol{u} = \boldsymbol{u}^{\text{pre}} \quad \text{on } \Gamma_{\text{D}}^{u},$$
 (4b)

$$\mathbf{P} \cdot \mathbf{N} = \mathbf{T}^{\text{pre}} \quad \text{on } \Gamma_{\text{N}}^{u}.$$
 (4c)

The weak form of the problem reads: Find $u \in \mathbb{U}$ that solves

$$\int_{\Omega} [\delta \boldsymbol{u} \otimes \nabla_{X}] : \boldsymbol{P}(\boldsymbol{F}) d\Omega = \int_{\Gamma_{N}^{\boldsymbol{u}}} \boldsymbol{T}^{\text{pre}} \cdot \delta \boldsymbol{u} d\Gamma \quad \forall \delta \boldsymbol{u} \in \mathbb{U}^{0},$$
 (5)

com/doi/10.1002/gamm.70010 by Chalmers University Of Technology, Wiley Online Library on [07/11/2025]. See the Terms

for the trial and test function spaces

$$\mathbb{U} = \{ \boldsymbol{u} \in [\mathbb{H}^1(\Omega)]^3 : \boldsymbol{u}|_{\Gamma_n^u} = \boldsymbol{u}^{\text{pre}} \}, \tag{6a}$$

$$\mathbb{U}^0 = \{ \boldsymbol{u} \in [\mathbb{H}^1(\Omega)]^3 : \boldsymbol{u}|_{\Gamma^u_D} = \boldsymbol{0} \}.$$
(6b)

Here, $\mathbb{H}^1(\bullet)$ denotes the Sobolev space of functions with square integrable 0^{th} and 1^{st} order derivatives.

2.3 | Fluid flow problem

For the deformed pore system, we shall now establish the seepage due to pressure gradients in the pore fluid. We consider the fluid pressure p, fluid velocity v and viscous stress $\sigma^{v}(v)$ with Stokes relation

$$\sigma^{\nu} = 2\mu [\nu \otimes \nabla]^{\text{sym}},\tag{7}$$

where ∇ is the nabla operator in the current configuration and μ is the dynamic viscosity of the fluid. To apply boundary conditions by prescribing a velocity \mathbf{v}^{pre} and traction \mathbf{t}^{pre} , the external boundary of the pore domain is split as $\gamma \cap \partial \omega^P = \gamma_{\text{D}}^{\nu} \cup \gamma_{\text{N}}^{\nu}$ into a Dirichlet part γ_{D}^{ν} and a Neumann part γ_{N}^{ν} .

The strong form of incompressible (cf. (8b)) Stokes flow in the current configuration can be stated as: Find $p:\omega\to\mathbb{R}$ and $v:\omega\to\mathbb{R}^3$ that solve

$$-\left[\boldsymbol{\sigma}^{\nu}(\boldsymbol{\nu}) - p\boldsymbol{I}\right] \cdot \boldsymbol{\nabla} = \mathbf{0} \quad \text{in } \omega^{P}, \tag{8a}$$

$$\mathbf{v} \cdot \mathbf{\nabla} = 0 \qquad \text{in } \omega^{\mathbf{P}}, \tag{8b}$$

$$v = v^{\text{pre}} \quad \text{on } \gamma_{\text{D}}^{v},$$
 (8c)

$$[\boldsymbol{\sigma}^{\boldsymbol{v}}(\boldsymbol{v}) - p\boldsymbol{I}] \cdot \boldsymbol{n} = \boldsymbol{t}^{\text{pre}} \quad \text{on } \gamma_{N}^{\boldsymbol{v}}, \tag{8d}$$

$$\mathbf{v} = \mathbf{0}$$
 on γ^{i} . (8e)

Next, we reformulate the problem in the reference configuration by i) expressing the current gradient in (8) as

$$[\diamondsuit \otimes \nabla] = [\diamondsuit \otimes \nabla_X] \cdot F^{-1}, \tag{9}$$

and ii) conducting a pull-back using Piola's identity

$$J[\diamondsuit \cdot \nabla] = \left[J \diamondsuit \cdot F^{-T} \right] \cdot \nabla_X. \tag{10}$$

Consequently, Stokes flow in the reference configuration can be stated as: Given v^{pre} , T^{pre} , F, find v and p that solve

$$-\left[\mathbf{P}^{v}(\mathbf{v},\mathbf{F})-pJ\mathbf{F}^{-T}\right]\cdot\mathbf{\nabla}_{X}=\mathbf{0}\qquad\text{in }\Omega^{P},$$
(11a)

$$JF^{-T}: [\mathbf{v} \otimes \nabla_X] = 0 \qquad \text{in } \Omega^P, \tag{11b}$$

$$\mathbf{v} = \mathbf{v}^{\text{pre}} \quad \text{on } \Gamma_{\text{D}}^{\text{v}},$$
 (11c)

$$\left[\mathbf{P}^{\nu}(\mathbf{v}, \mathbf{F}) - pJ\mathbf{F}^{-T} \right] \cdot \mathbf{N} = \mathbf{T}^{\text{pre}} \quad \text{on } \Gamma_{N}^{\nu}, \tag{11d}$$

$$\mathbf{v} = \mathbf{0}$$
 on Γ^{i} , (11e)

where the viscous part of the 1st Piola-Kirchhoff stress tensor reads*

$$P^{\nu}(\nu, F) = D(F) : [\nu \otimes \nabla_X], \tag{12a}$$

$$\mathbf{D}(\mathbf{F}) := J\mu \left[\mathbf{I} \otimes \left[\mathbf{F}^{-1} \cdot \mathbf{F}^{-T} \right] + \mathbf{F}^{-T} \otimes \mathbf{F}^{-1} \right]. \tag{12b}$$

^{*}We introduce the notation, $(\mathbf{A} \otimes \mathbf{B})_{ijkl} := A_{ik}B_{jl}, (\mathbf{A} \otimes \mathbf{B})_{ijkl} := A_{il}B_{jk}.$

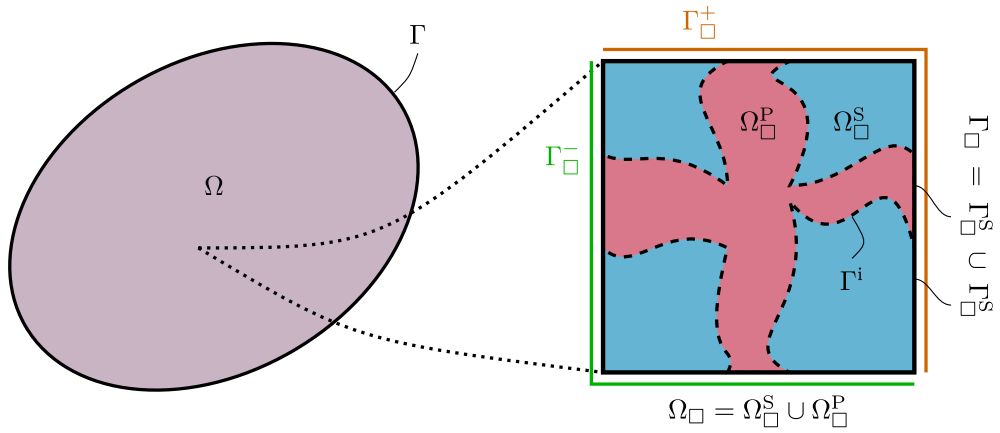


FIGURE 1 Schematic visualization of an RVE.

The weak form reads: Given v^{pre} , T^{pre} , F, find $v \in \mathbb{V}$ and $p \in \mathbb{P}$ that solve

$$\int_{\Omega^{P}} [\delta \boldsymbol{v} \otimes \boldsymbol{\nabla}_{X}] : [\boldsymbol{P}^{\nu}(\boldsymbol{v}, \boldsymbol{F}) - pJ\boldsymbol{F}^{-T}] d\Omega = \int_{\Gamma^{\nu}} \delta \boldsymbol{v} \cdot \boldsymbol{T}^{\text{pre}} d\Gamma \qquad \forall \delta \boldsymbol{v} \in \mathbb{V}^{0},$$
(13a)

$$\int_{\Omega^{\mathbb{P}}} \delta p J \mathbf{F}^{-T} : [\mathbf{v} \otimes \nabla_X] d\Omega = 0 \qquad \forall \delta p \in \mathbb{P},$$
(13b)

for the trial and test function spaces

$$\mathbb{V} = \{ \boldsymbol{\nu} \in [\mathbb{H}^1(\Omega^P)]^3 : \boldsymbol{\nu}|_{\Gamma_D^{\nu}} = \boldsymbol{\nu}^{\text{pre}}, \boldsymbol{\nu}|_{\Gamma^i} = \boldsymbol{0} \}, \tag{14a}$$

$$\mathbb{V}^0 = \{ \boldsymbol{\nu} \in [\mathbb{H}^1(\Omega^P)]^3 : \boldsymbol{\nu}|_{\Gamma_p^{\nu}} = \boldsymbol{0}, \boldsymbol{\nu}|_{\Gamma^i} = \boldsymbol{0} \}, \tag{14b}$$

$$\mathbb{P} = \mathbb{L}_2(\Omega^P). \tag{14c}$$

3 | VARIATIONALLY CONSISTENT HOMOGENIZATION

3.1 | Preliminaries

Homogenization is carried out on given realization of the microstructure, defined by an RVE; however, whether the RVE is actually representative is not an issue in this article. We denote the RVE domain Ω_{\square} , Γ_{\square} is its boundary, $(\Omega_{\square}^S, \Omega_{\square}^P, \Gamma_{\square}^P)$ are associated with the corresponding phases, and Γ_{\square}^i is their interface. A visualization of the RVE is given in Figure 1. Note that, although it could not be visualized in Figure 1, both Ω_{\square}^S , Ω_{\square}^P are assumed to be continuous.

Volume and surface averages of an intensive field ♦ are defined as

$$\langle \diamond \rangle_{\square}^{S} := \frac{1}{|\Omega_{\square}|} \int_{\Omega_{\square}^{S}} \diamond d\Omega, \quad \langle \diamond \rangle_{\square}^{P} := \frac{1}{|\Omega_{\square}|} \int_{\Omega_{\square}^{P}} \diamond d\Omega, \quad \langle \diamond \rangle_{\square} := \langle \diamond \rangle_{\square}^{S} + \langle \diamond \rangle_{\square}^{P}, \tag{15a}$$

$$\langle \diamond \rangle^{S} := \frac{1}{|\Omega_{\square}^{S}|} \int_{\Omega_{\square}^{S}} \diamond d\Omega, \quad \langle \diamond \rangle^{P} := \frac{1}{|\Omega_{\square}^{P}|} \int_{\Omega_{\square}^{P}} \diamond d\Omega, \tag{15b}$$

$$\langle\!\langle \diamond \rangle\!\rangle_{\square} := \frac{1}{|\Omega_{\square}|} \int_{\Gamma_{\square}} \diamond d\Gamma.$$
 (15c)

The macroscale representation of a quantity \diamond is denoted $\overline{\diamond}$.

For a mirror point $X \in \Gamma_{\square}^+$ and the corresponding image point $X^-(X) \in \Gamma_{\square} \setminus \Gamma_{\square}^+$, we define the RVE jump operator $[\![\bullet]\!]_{\square}(X) := \bullet(X) - \bullet(X^-(X))$.

3.2 | Mechanical problem

The mechanical RVE problem can be derived as presented in [19]: Given \overline{F} , find $u \in \mathbb{U}_{\square}$ and $\lambda \in \mathbb{L}_{\square}$ that solve

$$\langle \mathbf{P}(\mathbf{u}) : [\delta \mathbf{u} \otimes \nabla_X] \rangle_{\square} - \frac{1}{|\Omega_{\square}|} \int_{\Gamma_{\square}^+} \lambda \cdot [\![\delta \mathbf{u}]\!]_{\square} d\Gamma = 0 \qquad \forall \delta \mathbf{u} \in \mathbb{U}_{\square}, \qquad (16a)$$

$$-\frac{1}{|\Omega_{\square}|} \int_{\Gamma_{\square}^{+}} \delta \lambda \cdot [\![\boldsymbol{u}]\!]_{\square} d\Gamma = -\frac{1}{|\Omega_{\square}|} \int_{\Gamma_{\square}^{+}} \lambda \otimes [\![\boldsymbol{X} - \overline{\boldsymbol{X}}]\!]_{\square} d\Gamma : [\overline{\boldsymbol{F}} - \boldsymbol{I}] \qquad \forall \delta \lambda \in \mathbb{L}_{\square}, \tag{16b}$$

with the trial and test function spaces

$$\mathbb{U}_{\square} = \{ \boldsymbol{u} \in [\mathbb{H}^{1}(\Omega_{\square})]^{3} : \langle \langle \boldsymbol{u} \rangle \rangle_{\square} = \boldsymbol{0} \}, \tag{17a}$$

$$\mathbb{L}_{\square} = [\mathbb{L}_2(\Gamma_{\square}^+)]^3. \tag{17b}$$

3.3 | Fluid flow problem

3.3.1 | Two-scale problem

Firstly, we introduce running averages into the weak form equations. The fluid flow problem now reads:

$$\int_{\Omega^{P}} \langle [\delta \boldsymbol{v} \otimes \boldsymbol{\nabla}_{X}] : [\boldsymbol{P}^{\nu}(\boldsymbol{v}, \boldsymbol{F}) - pJ\boldsymbol{F}^{-T}] \rangle_{\square} d\Omega = \int_{\Gamma_{\nu}^{\nu}} \delta \boldsymbol{v} \cdot \boldsymbol{T}^{\text{pre}} d\Gamma \quad \forall \delta \boldsymbol{v} \in \mathbb{V}^{0},$$
(18a)

$$\int_{\Omega^{P}} \langle \delta p J \mathbf{F}^{-T} : [\mathbf{v} \otimes \mathbf{\nabla}_{X}] \rangle_{\square} d\Omega = 0 \qquad \forall \delta p \in \mathbb{P}^{0}.$$
 (18b)

Then, we assume the additive decomposition of the pressure in macroscale contribution p^{M} and sub-scale fluctuation part p^{s} .

$$p = p^{\mathcal{M}} + p^{\mathcal{S}}. \tag{19}$$

Moreover, we utilize a linear prolongation of the homogenized macroscale pressure \overline{p} and its gradient $\overline{G}:=\nabla_X\overline{p}$

$$p^{\mathrm{M}}[\overline{p}] = \overline{p}(\overline{X}) + \overline{G}(\overline{X}) \cdot [X - \overline{X}^{\mathrm{P}}] \qquad \text{for } X \in \Omega_{\square}^{\mathrm{P}}(\overline{X}), \tag{20}$$

where $\overline{X}^{P} = \langle X \rangle^{P}$.

Next, we define the homogenization operators

$$\overline{p}_{\square}[p] := \langle p \rangle^{P}, \tag{21a}$$

$$\overline{\boldsymbol{G}}_{\square}[p] := \int_{\Gamma_{\square}^{P,+}} [\![p]\!]_{\square} \boldsymbol{N} d\Gamma \cdot \left[\int_{\Gamma_{\square}^{P,+}} [\![\boldsymbol{X} - \overline{\boldsymbol{X}}]\!]_{\square} \otimes \boldsymbol{N} d\Gamma \right]^{-1}, \tag{21b}$$

and introduce the constraints

$$\overline{p}_{\square}[p^{\mathrm{s}}] = 0, \tag{22a}$$

$$\overline{G}_{\square}[p^s] = \mathbf{0}.\tag{22b}$$

By incorporating the decomposition of the pore pressure in (19) with (20), we ensure that $\overline{p}_{\square}[p] = \overline{p}$ and $\overline{G}_{\square}[p] = \overline{g}$ holds. In order to show this result, we use the identities $\overline{p}_{\square}[p^M] = \overline{p}$ and $\overline{G}_{\square}[p^M] = \overline{G}$ together with the constraints (22a,b).

To apply boundary conditions, we decompose the external part of the pore space boundary into Dirichlet and Neumann parts as $\Gamma \cap \partial \Omega^P = \Gamma^{\nu}_D \cup \Gamma^{\nu}_N$. Further, we express the applied tractions in terms of their fluctuation part as $T^s = T + \underline{p}^M J F^{-T} \cdot N$. The weak form of the fluid flow problem then reads: Given $T^{s, \text{pre}}$, v^{pre} , $\overline{p}^{\text{pre}}$, F, find $v \in V$, $p^s \in \mathbb{P}^s$ and $\overline{p} \in \mathbb{P}$ that solve

$$\int_{\Omega^{\mathbf{P}}} \langle [\delta \boldsymbol{v} \otimes \boldsymbol{\nabla}_{X}] : [\boldsymbol{P}^{\mathbf{v}}(\boldsymbol{v}, \boldsymbol{F}) - p^{s} J \boldsymbol{F}^{-T}] + \delta \boldsymbol{v} \cdot J \boldsymbol{F}^{-T} \cdot [\boldsymbol{\nabla}_{X} p^{\mathbf{M}}[\overline{p}]] \rangle_{\square} d\Omega = \int_{\Gamma_{\mathbf{N}}^{\mathbf{v}}} \delta \boldsymbol{v} \cdot \boldsymbol{T}^{s, \text{pre}} d\Gamma \quad \forall \delta \boldsymbol{v} \in \mathbb{V}^{0},$$
(23a)

$$\int_{\Omega^{\mathbf{P}}} \langle \delta p^{\mathbf{s}} J \mathbf{F}^{-T} : [\mathbf{v} \otimes \mathbf{\nabla}_{X}] \rangle_{\square} d\Omega = 0 \qquad \forall \delta p^{\mathbf{s}} \in \mathbb{P}^{\mathbf{s}}, \tag{23b}$$

$$-\int_{\Omega^{\mathbf{P}}} \langle \boldsymbol{v} \cdot J \boldsymbol{F}^{-T} \cdot \left[\boldsymbol{\nabla}_{X} p^{\mathbf{M}} [\delta \overline{p}] \right] \rangle_{\square} d\Omega = -\int_{\Gamma_{\mathbf{D}}^{\mathbf{P}}} p^{\mathbf{M}} [\delta \overline{p}] \boldsymbol{v}^{\mathbf{pre}} \cdot J \boldsymbol{F}^{-T} \cdot \boldsymbol{N} d\Gamma \qquad \forall \delta \overline{p} \in \overline{\mathbb{P}}^{0}, \tag{23c}$$

for the trial and test function spaces

$$\mathbb{V} = \{ \boldsymbol{\nu} \in [\mathbb{H}^1(\Omega^P)]^3 : \boldsymbol{\nu}|_{\Gamma_D^{\nu}} = \boldsymbol{\nu}^{\text{pre}}, \boldsymbol{\nu}|_{\Gamma^i} = \boldsymbol{0} \}, \tag{24a}$$

$$\mathbb{V}^{0} = \{ \boldsymbol{\nu} \in [\mathbb{H}^{1}(\Omega^{P})]^{3} : \boldsymbol{\nu}|_{\Gamma_{D}^{\nu}} = \mathbf{0}, \boldsymbol{\nu}|_{\Gamma^{i}} = \mathbf{0} \}, \tag{24b}$$

$$\mathbb{P}^{\mathbf{s}} = \{ p \in \mathbb{H}^1(\Omega^{\mathbf{P}}) : \overline{p}_{\square}[p|_{\Omega^{\mathbf{P}}_{\square}}] = 0, \overline{G}_{\square}[p|_{\Omega^{\mathbf{P}}_{\square}}] = \mathbf{0} \}, \tag{24c}$$

$$\overline{\mathbb{P}} = \{ p \in \mathbb{H}^1(\Omega^P) : p|_{\Gamma_N^v} = \overline{p}^{\text{pre}} \}, \tag{24d}$$

$$\overline{\mathbb{P}}^{0} = \{ p \in \mathbb{H}^{1}(\Omega^{P}) : p|_{\Gamma_{\bullet}^{V}} = 0 \}.$$
 (24e)

Remark 1. By choosing the homogenization operators (21a,b), we (implicitly) require higher regularity of the pore pressure, seeking $p \in \mathbb{H}^1(\Omega^P) \subset \mathbb{L}_2(\Omega^P)$.

3.3.2 | Macroscale problem

By choosing $\delta p^s = 0$ and $\delta v = 0$ we obtain the macroscale problem: Given \overline{W}^{pre} and \overline{p}^{pre} , find $\overline{p} \in \overline{\mathbb{P}}$ that solves

$$-\int_{\overline{\Omega}} \overline{\boldsymbol{W}} \cdot [\boldsymbol{\nabla}_{X} \delta \overline{p}] d\Omega = -\int_{\overline{\Gamma}_{N}} \delta \overline{p} \overline{\boldsymbol{W}}^{\text{pre}} d\Gamma \quad \forall \delta \overline{p} \in \overline{\mathbb{P}}^{0},$$
(25)

with the trial and test function spaces

$$\overline{\mathbb{P}} = \{ p \in \mathbb{H}^1(\Omega) : p|_{\overline{\Gamma}_D} = \overline{p}^{\text{pre}} \}, \tag{26a}$$

$$\overline{\mathbb{P}}^0 = \{ p \in \mathbb{H}^1(\Omega) : p|_{\overline{\Gamma}_D} = 0 \}, \tag{26b}$$

and the effective Piola seepage

$$\overline{\boldsymbol{W}} = \langle \boldsymbol{v} \cdot J \boldsymbol{F}^{-T} \rangle_{\square}^{P}. \tag{27}$$

3.3.3 | RVE problem

By choosing $\delta \overline{p} = 0$ we obtain the RVE problem for periodic boundary conditions: Given F and \overline{G} , find $v \in \mathbb{V}_{\square}$ and $p^s \in \mathbb{P}_{\square}$ that solve

$$\langle [\delta \boldsymbol{v} \otimes \boldsymbol{\nabla}_{X}] : \boldsymbol{D}(\boldsymbol{F}) : [\boldsymbol{v} \otimes \boldsymbol{\nabla}_{X}] \rangle_{\square}^{P} - \langle p^{s} J \boldsymbol{F}^{-T} : [\delta \boldsymbol{v} \otimes \boldsymbol{\nabla}_{X}] \rangle_{\square}^{P} = -\langle \delta \boldsymbol{v} \cdot J \boldsymbol{F}^{-T} \rangle_{\square}^{P} \cdot \overline{\boldsymbol{G}} \qquad \forall \delta \boldsymbol{v} \in \mathbb{V}_{\square},$$
(28a)

$$-\left\langle \delta p^{s} J \mathbf{F}^{-T} : [\mathbf{v} \otimes \mathbf{\nabla}_{X}] \right\rangle_{\square}^{P} = 0 \qquad \forall \delta p^{s} \in \mathbb{P}_{\square}, \tag{28b}$$

doi/10.1002/gamm.70010 by Chalmers University Of Technology, Wiley Online Library on [07/11/2025]. See

with trial and test function spaces

$$\mathbb{V}_{\square} = \{ \boldsymbol{v} \in [\mathbb{H}^{1}(\Omega^{P})]^{3} : \boldsymbol{v}|_{\Gamma_{\square}^{i}} = \boldsymbol{0}, [[\boldsymbol{v}]]_{\square} = \boldsymbol{0} \text{ on } \Gamma_{\square}^{P,+} \},$$
(29a)

$$\mathbb{P}_{\square} = \{ p \in \mathbb{H}^{1}(\Omega^{P}) : \overline{p}_{\square}[p] = 0, [[p]]_{\square} = 0 \text{ on } \Gamma_{\square}^{P,+} \}.$$
 (29b)

Remark 2. Since the constraint $\overline{G}_{\square}[p^s] = \mathbf{0} \quad \forall p^s \in \mathbb{P}_{\square}$ is automatically satisfied by the choice of periodic boundary conditions, it is not explicitly imposed in (29b).

4 | UPSCALING

Since the Stokes flow problem for a given deformation F is linear in v and p, the effective flow properties can be computed once and for all by direct upscaling via unit loadings and sensitivities. We can express the effective seepage in a format according to Darcy's law

$$\overline{W} = -\overline{K} \cdot \overline{G},\tag{30}$$

where \overline{K} is the effective permeability tensor for a specific deformation F. Next, we define $(\hat{v}^{(i)}, \hat{p}^{s(i)})$ as the solution of the RVE-problem (28) for a unit loading $\overline{G} = e_i$. For given F, we seek $\hat{v}^{(i)}\{F\} \in \mathbb{V}_{\square}$, $\hat{p}^{s(i)}\{F\} \in \mathbb{P}_{\square}$, such that for $i \in \{1, 2, 3\}$

$$\left\langle \left[\delta \boldsymbol{v} \otimes \boldsymbol{\nabla}_{X} \right] : \boldsymbol{D}(\boldsymbol{F}) : \left[\hat{\boldsymbol{v}}^{(i)} \otimes \boldsymbol{\nabla}_{X} \right] \right\rangle_{\square}^{P} - \left\langle \hat{p}^{S(i)} J \boldsymbol{F}^{-T} : \left[\delta \boldsymbol{v} \otimes \boldsymbol{\nabla}_{X} \right] \right\rangle_{\square}^{P} = - \left\langle \delta \boldsymbol{v} \cdot J \boldsymbol{F}^{-T} \right\rangle_{\square}^{P} \cdot \boldsymbol{e}_{i} \quad \forall \delta \boldsymbol{v} \in \mathbb{V}_{\square}, \tag{31a}$$

$$-\left\langle \delta p^{s} J \mathbf{F}^{-T} : \left[\hat{\mathbf{v}}^{(i)} \otimes \mathbf{\nabla}_{X} \right] \right\rangle_{\square}^{P} = 0 \qquad \forall \delta p^{s} \in \mathbb{P}_{\square}, \qquad (31b)$$

Now, we may express the velocity field as

$$\mathbf{v} = \left[\sum_{i} \hat{\mathbf{v}}^{(i)} \otimes \mathbf{e}_{i} \right] \cdot \overline{\mathbf{G}}. \tag{32}$$

Finally, the effective permeability can be computed as

$$\overline{K} = \sum_{i} - \langle \hat{\mathbf{v}}^{(i)} \cdot J \mathbf{F}^{-T} \rangle_{\square}^{P} \otimes \mathbf{e}_{i} = \sum_{i,j} \left\langle [\hat{\mathbf{v}}^{(i)} \otimes \nabla_{X}] : \mathbf{D}(\mathbf{F}) : [\hat{\mathbf{v}}^{(j)} \otimes \nabla_{X}] \right\rangle_{\square}^{P} \mathbf{e}_{i} \otimes \mathbf{e}_{j}.$$
(33)

In order to show the first identity in (33), we insert (32) into the definition (27) of the effective seepage and rearrange the result into a format matching (30). To show the second identity, from which it appears that \overline{K} is symmetrical, we argue as follows: Set $\delta v = \hat{v}^{(j)}$ in (28a) and $\delta p^s = \hat{p}^{s(j)}$ in (28b) to obtain the identity

$$\left(\overline{\boldsymbol{K}}\right)_{ij} = -\left\langle \hat{\boldsymbol{v}}^{(j)} \cdot J\boldsymbol{F}^{-T} \right\rangle_{\square}^{P} \cdot \boldsymbol{e}_{i} = \left\langle \left[\hat{\boldsymbol{v}}^{(j)} \otimes \boldsymbol{\nabla}_{X}\right] : \boldsymbol{D}(\boldsymbol{F}) : \left[\hat{\boldsymbol{v}}^{(i)} \otimes \boldsymbol{\nabla}_{X}\right] \right\rangle_{\square}^{P}.$$
(34)

5 | NUMERICAL STUDY

5.1 | Preliminaries

We consider artificially generated unit cells according to the procedure presented in [7]. We consider periodic unit cells, which, for the sake of simplicity, we refer to as RVEs. For the matrix material, we choose the Lamé constants $\lambda = 84$ GPa and G = 38 GPa (see A), whereas for the pore space we use $\lambda = 8.4$ MPa, G = 3.8 MPa together with the viscosity $\mu = 1$ mPa · s (approximating water at room temperature).

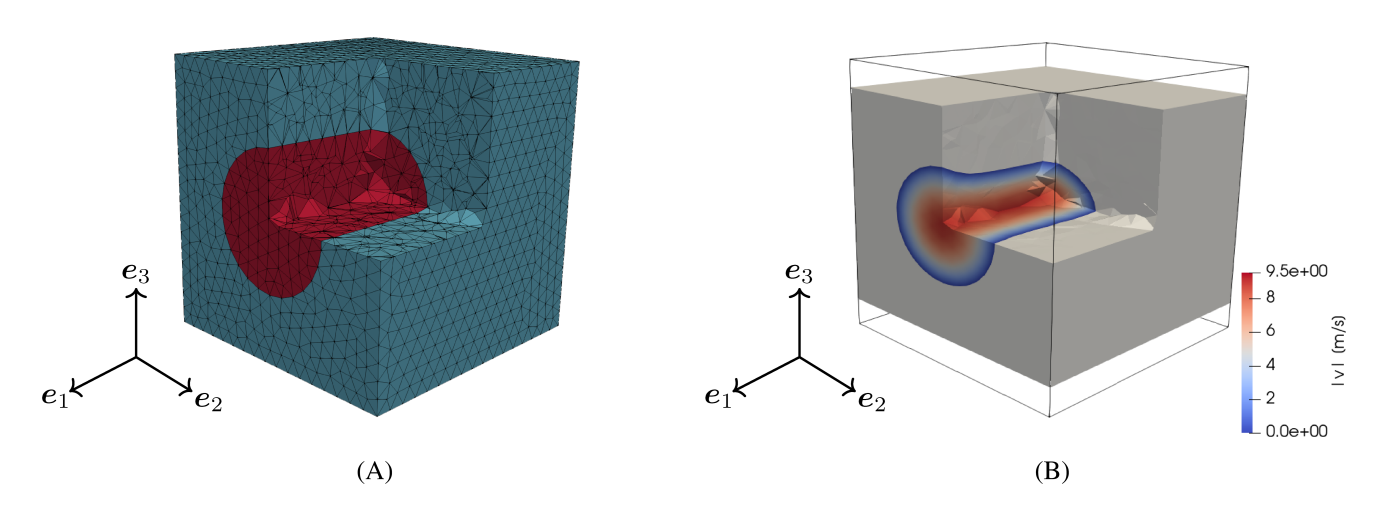
The numerical results are obtained using the Finite Element tool box Ferrite.jl [6]. For the mechanical problem (16a,b), linear tetrahedral elements are used for the displacement field. As a special case of periodicity, Dirichlet boundary conditions are applied. For the fluid flow problem (31a,b), Taylor-Hood elements are used for pressure and velocity.

Simple RVE with a single cylindrical pore 5.2

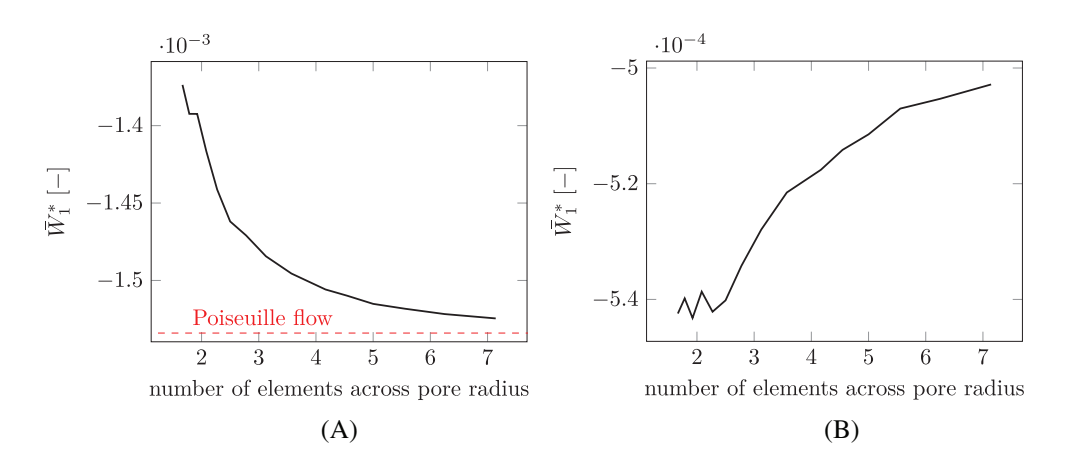
As the first validation of the method, we consider a simple RVE with a single cylindrical pore aligned with the x_1 -axis. The edge length of the RVE is $l_{RVE} = 1$ m and the pore radius is r = 0.25 m. For different mesh resolutions, the effective seepage velocity in pore direction \overline{W}_1 resulting from a pressure gradient of 1 $\frac{Pa}{m}$ in pore direction is computed. As mechanical loading, compression to $\overline{F}_{33}=0.8$ is applied. More specifically, macroscale deformation gradients are prescribed with $\overline{F}_{11} = \overline{F}_{22} = 1$ and $\overline{F}_{ij} = 0$ for $i \neq j$. The remaining component \overline{F}_{33} is varied from 1 to 0.8 in load steps. In Figure 2, a visualization of the undeformed and deformed RVE with an average mesh size of $l_{\text{mesh}} = 0.055$ m is given.

For all mesh resolutions, the resulting seepage velocities in the undeformed and the deformed state are collected in Figure 3. For the undeformed RVE, an analytical reference solution can be derived assuming Poiseuille flow.

For increasing mesh resolution, we observe convergence of the effective seepage velocity in the undeformed RVE to the reference value from Poiseuille flow (cf. Figure 3a). In Figure 3b, for the deformed RVE, one can observe convergence towards a value of \overline{W}_1 which is approximately 33% of the corresponding value in the undeformed RVE. The great influence of the deformation on the effective permeability can be explained by the change in pore cross section area. The pore cross



RVE with a single cylindrical pore in the undeformed state and for $\overline{F}_{33} = 0.8$. The average mesh size is $l_{\text{mesh}} = 0.055$ m which corresponds to 4.55 elements across the pore radius r = 0.25 m, (A) Undeformed RVE mesh. The pore space is colored red and the surrounding matrix light blue. (B) Deformed RVE with velocity magnitude in the pore space. The matrix is colored light gray.



Mesh convergence study: Non-dimensional effective seepage velocity $\overline{W}_1^* = \frac{\mu}{l_{\text{RVE}}^2 \overline{G}} \overline{W}_1$ through an RVE with a single cylindrical pore for a pressure gradient of magnitude $\overline{G} = 1$ $\frac{Pa}{m}$ (giving $\overline{W}_1^* = 10^{-3} \frac{s}{m} \cdot \overline{W}_1$) in pore direction and different mesh resolutions. The mesh resolution is quantified by the average number of elements across the pore radius computed from the average mesh size, (A) Undeformed RVE. (B) Deformed RVE for compression to $\overline{F}_{33} = 0.8$.

FIGURE 4 Example of an RVE in the undeformed state and for $\overline{F}_{33} = 0.8$. The pore space is colored red and the surrounding matrix light blue, (A) Undeformed RVE. (B) Deformed RVE.

section greatly influences the fluid flow velocity due to the no-slip condition on the interface to the solid skeleton and the resulting quadratic velocity profile.

Furthermore, for a coarse mesh resolution, we observe that \overline{W}_1 in the undeformed RVE is underestimated while in the deformed RVE it is overestimated. The latter can be explained by an underestimation of the deformation. Overall, this indicates that the ratio of effective permeability in the deformed and undeformed configuration is likely to be overestimated.

For the following study of more complex RVEs we consider 3 to 4 elements across the mean pore radius to be sufficient for the purpose of demonstrating the presented method. Although we do not quantify the pore size, we try to choose the mesh resolution accordingly.

5.3 | Complex RVEs under uniaxial compression

Next, sets of statistically generated RVEs with a more complex microstructure are considered under uniaxial compression. The same compressive loading as in the previous Section is applied to the mechanical problem (16a,b) and the resulting deformation is used in the fluid flow problem (31a,b). An example RVE in the initial and final configuration is depicted in Figure 4. For these two states, the magnitude of the fluid velocity in the pore space is depicted in Figure 5.

It can be observed that the compression significantly reduces the pore size. Moreover, for the same pressure gradient, the fluid velocity in the deformed material is significantly smaller than in the undeformed state. This indicates a great influence of the deformation on the effective permeability.

To study the effective permeability, sets of 10 RVEs are investigated. All RVEs have the same size $l_{\text{RVE}} = 1 \, \mu \text{m}$ and mesh resolution $l_{\text{mesh}} = 0.045 \pm 0.005 \, \mu \text{m}$. Each set contains RVEs with a certain porosity $n_{\text{P}} \in \{40\%, 50\%, 60\%\}$.

When applying the compression, the effective permeability is computed for some of the load steps from (31a,b) and (33). The resulting components of \overline{K} are depicted in Figure 6 and normalized values are presented in Figure 7.

The values in Figure 6 for $\overline{F}_{33} = 1$ confirm the expectation that the permeability in the undeformed state is isotropic and increases significantly with the porosity. Interestingly, the relative change during deformation is very similar upon changing porosity (cf. Figure 7).

Due to the uniaxial loading, the change in permeability is strongly anisotropic. For a compression of 20% strain, orthogonal to the compression direction a decrease of permeability of almost 60% can be observed while in compression direction the decrease is about 20%. The decrease in permeability orthogonal to the compression direction is about three times larger than in compression direction. This is plausible, as the applied loading directly reduces the cross section area of pores which are aligned orthogonal to the compression direction, while pores aligned with the compression direction are influenced by transverse expansion effects: The RVE as a whole is prescribed to have no effective transverse expansion, however, the matrix material inside is allowed to expand into the pore space. Note that upon computing effective permeabilities in a kinematically nonlinear description covers 2 effects: (1) Reducing the pore size and, hence, the geometric permeability of the structure; (2) changing the RVE length (in our case in e_3 -direction) which is influencing the length

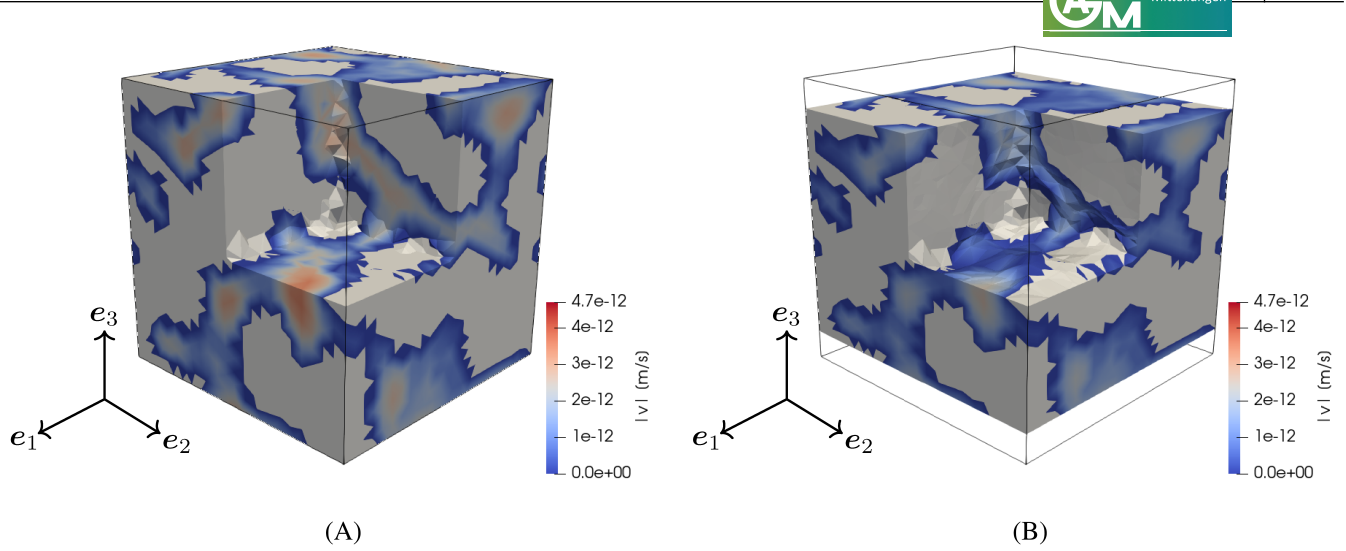


FIGURE 5 Velocity magnitude ||v|| in the pore space of an example RVE in the undeformed state and for $\overline{F}_{33} = 0.8$ resulting from a pressure gradient $\overline{G} = e_1 \frac{Pa}{m}$. The matrix is colored light gray, (A) Undeformed RVE. (B) Deformed RVE.

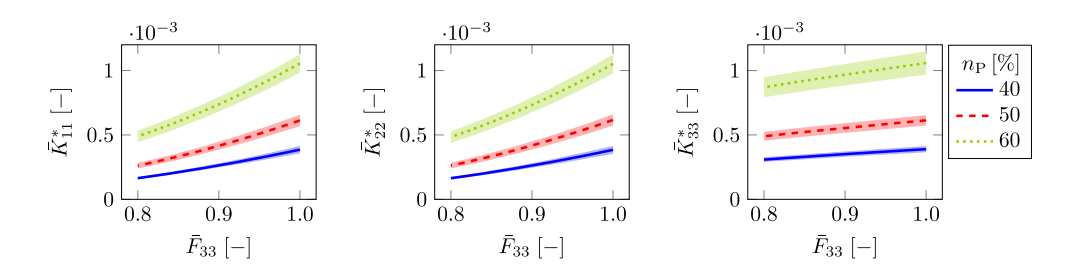


FIGURE 6 Non-dimensional components of the effective permeability tensor \overline{K} versus the applied deformation for sets of 10 RVEs. Each set is characterized by a different porosity $n_{\rm P}$. The lines represent the mean values of the sets and the shaded areas around them visualize the standard deviation. The non-dimensional components are computed as $\overline{K}_{ij}^* = \frac{\mu}{l_{\rm RVE}^2} \overline{K}_{ij}$ with $\frac{\mu}{l_{\rm RVE}^2} = 10^9 \frac{\rm Pa\cdot s}{\rm m^2}$ in this example.

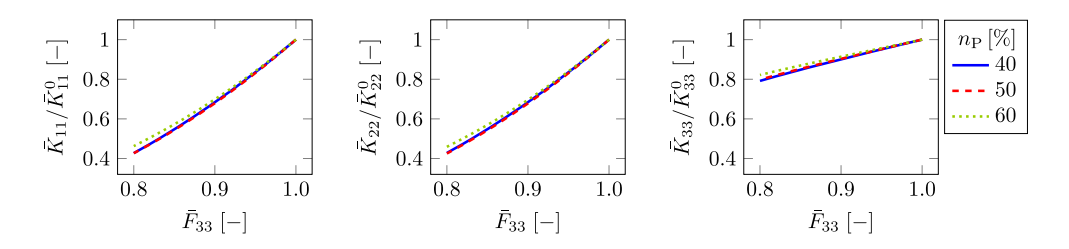


FIGURE 7 Normalized components of the effective permeability tensor \overline{K} versus the applied deformation for sets of 10 RVEs. Each set is characterized by a different porosity n_P . The values are normalized with the components of \overline{K}^0 as the effective permeability tensor of the corresponding undeformed RVE. The lines represent the mean values of the sets.

on which the pressure gradient is acting. The first effect decreases permeability perpendicular to compression direction, the latter increases effective permeability in loading direction.

6 | CONCLUSION

In this article, we have developed a procedure for computing the deformation-dependent effective permeability of a bicontinuous porous material. The deformation is computed in a finite strain setting applying a compressible Neo-Hookean

.5222608, 2025, 4, Downloaded from https://onlinelibrary.wiley.com/doi/10.1002/gamm.70010 by Chalmers University Of Technology, Wiley Online Library on [07/11/2025]. See the Terms

on Wiley Online Library for rules of use; OA articles are governed by the applicable Creative Commons

material model. The influence of the pore pressure on the deformation was neglected. Instead, the pore space was considered a fictitious, soft, elastic solid. This way, self-penetration of the matrix is prevented and the resulting deformation of the pore space can conveniently applied to the second problem. Fluid flow in the deformed pore space was expressed in terms of a Stokes flow model. The computed deformation was accounted for by using the resulting deformation gradient for a pull-back operation.

The VCH framework was employed to derive an upscaling scheme based on a set of numerically generated RVEs representing the microstructure. To efficiently compute the deformation-dependent effective permeability, a two-step procedure was developed using a third-medium approach to accommodate large deformations of the pore system. In the first step, the deformation of each RVE is determined for a given macroscale deformation gradient. In the second step, the linear nature of the flow problem at fixed deformation is exploited to evaluate the effective permeability from the sensitivities of the velocity field with respect to macroscale pressure gradients.

A numerical study was conducted on a set of RVEs with similar porosity and the same material parameters. Uniaxial compression was considered to investigate the influence of the deformation on the effective permeability. A significant reduction of effective permeability was observed for a compression up to 20% strain: In compression direction the reduction was about 20% and in orthogonal directions about 60%.

The great influence of the deformation motivates further research for accurate prediction of the effective permeability. A natural next step would be the extension of the presented one-way coupled approach to a fully coupled model. The fluid traction (from the fluid pressure) will then be correctly accounted for at the computation of the deformed porous skeleton and porespace. Obviously, this calls for an iterative procedure. Moreover, a validation with experimental data would be valuable.

ACKNOWLEDGEMENTS

This research was funded by the Swedish Research Council (VR) via grant Nos. 2020-05057 and 2024-05854, which is gratefully acknowledged. Open Access funding enabled and organized by Projekt DEAL.

DATA AVAILABILITY STATEMENT

The data that support the findings of this study are available from the corresponding author upon reasonable request.

ORCID

David René Rollin https://orcid.org/0000-0001-9119-9577
Fredrik Larsson https://orcid.org/0000-0002-7786-5040
Kenneth Runesson https://orcid.org/0000-0003-1714-4994
Ralf Jänicke https://orcid.org/0000-0001-8816-6643

REFERENCES

- [1] Y. Amirat, V. Shelukhin, and K. Trusov, Flows of two slightly miscible fluids in porous media: Two-scale numerical modeling, Transp. Porous Media 151 (2024), no. 6, 1423–1452. https://doi.org/10.1007/s11242-024-02080-1.
- [2] S. Arbabi and M. Sahimi, The transition from darcy to nonlinear flow in heterogeneous porous media: I single-phase flow, Transp. Porous Media **151** (2024), no. 4, 795–812. https://doi.org/10.1007/s11242-024-02070-3.
- [3] J. W. Arblaster, Densities of osmium and iridium, Platin. Met. Rev. 33 (1989), no. 1, 14-16. https://doi.org/10.1595/003214089X3311416.
- [4] R. Arbter, J. Beraud, C. Binetruy, L. Bizet, J. Bréard, S. Comas-Cardona, C. Demaria, A. Endruweit, P. Ermanni, F. Gommer, S. Hasanovic, P. Henrat, F. Klunker, B. Laine, S. Lavanchy, S. Lomov, A. Long, V. Michaud, G. Morren, E. Ruiz, H. Sol, F. Trochu, B. Verleye, M. Wietgrefe, W. Wu, and G. Ziegmann, Experimental determination of the permeability of textiles: A benchmark exercise, Compos. Part A Appl. Sci. Manuf. 42 (2011), no. 9, 1157–1168. https://doi.org/10.1016/j.compositesa.2011.04.021.
- [5] S. Brundiers, P. Trinke, B. Bensmann, and R. Hanke-Rauschenbach, Model-based investigation of recombination interlayers in PEM water electrolysis: Concentration profiles, efficiency, and operational limits, J. Electrochem. Soc. **171** (2024), no. 7, 074509. https://doi.org/10.1149/1945-7111/ad6212.
- [6] K. Carlsson, F. Ekre, Ferrite. JI contributors, https://github.com/Ferrite-FEM/Ferrite.jl
- [7] D. Carolan, H. Chong, A. Ivankovic, A. Kinloch, and A. Taylor, Co-continuous polymer systems: A numerical investigation, Comput. Mater. Sci. 98 (2015), 24–33. https://doi.org/10.1016/j.commatsci.2014.10.039.
- [8] L. Chaabane, L. Dammak, D. Grande, C. Larchet, P. Huguet, S. Nikonenko, and V. Nikonenko, Swelling and permeability of Nafion® 117 in water-methanol solutions: An experimental and modelling investigation, J. Membr. Sci. 377 (2011), no. 1, 54–64. https://doi.org/10.1016/j.memsci.2011.03.037.

.5222608, 2025, 4, Downloaded from https://onlinelibrary.wiley.com/doi/10.1002/gamm.70010 by Chalmers University Of Technology, Wiley Online Library on [07/11/2025]. See the Terms and Condit

Online Library for rules of use; OA articles are governed by the applicable Creative Common

- [9] O. Faltus, M. Horák, M. Doškář, and O. Rokoš, Third medium finite element contact formulation for pneumatically actuated systems, Comput. Methods Appl. Mech. Eng. **431** (2024), 117262. https://doi.org/10.1016/j.cma.2024.117262.
- [10] E. A. Franceschini and H. R. Corti, Elastic properties of Nafion, polybenzimidazole and poly [2,5-benzimidazole] membranes determined by AFM tip nano-indentation, J. Power Sources **188** (2009), no. 2, 379–386. https://doi.org/10.1016/j.jpowsour.2008.12.019.
- [11] B. Guo, R. Yu, Z. Zhang, Y. Wang, and D. Niu, Numerical model of chloride reactive transport in concrete a review, Transp. Porous Media 151 (2024), no. 2, 367–398. https://doi.org/10.1007/s11242-023-02053-w.
- [12] L. B. Hunt, A history of iridium, Platin. Met. Rev. 31 (1987), no. 1, 32-41. https://doi.org/10.1595/003214087X3113241.
- [13] T. Krenz, A. Rex, L. Helmers, P. Trinke, B. Bensmann, and R. Hanke-Rauschenbach, Reversible degradation phenomenon in PEMWE cells: An experimental and modeling study, J. Electrochem. Soc. 171 (2024), no. 12, 124501. https://doi.org/10.1149/1945-7111/ad96e4.
- [14] S.-F. Lu, Z.-J. Han, L. Xu, T.-G. Lan, X. Wei, and T.-Y. Zhao, On measuring methods and influencing factors of air permeability of soils: An overview and a preliminary database, Geoderma 435 (2023), 116509. https://doi.org/10.1016/j.geoderma.2023.116509.
- [15] C. C. Mei and J.-I. Auriault, Mechanics of heterogeneous porous media with several spatial scales, Proc. R. Soc. Lon. A 426 (1989), 391–423. https://doi.org/10.1098/rspa.1989.0132.
- [16] F. Pennella, G. Cerino, D. Massai, D. Gallo, G. F. D'Urso Labate, A. Schiavi, M. A. Deriu, A. Audenino, and U. Morbiducci, A survey of methods for the evaluation of tissue engineering scaffold permeability, Ann. Biomed. Eng. 41 (2013), 2027–2041. https://doi.org/10.1007/s10439-013-0815-5.
- [17] Ph. Renard and G. de Marsily, Calculating equivalent permeability: a review, Adv. Water Resour. 20 (1997), no. 5, 253–278. https://doi.org/10.1016/S0309-1708(96)00050-4.
- [18] C. Sandström, F. Larsson, K. Runesson, and H. Johansson, A two-scale finite element formulation of stokes flow in porous media, Comput. Methods Appl. Mech. Eng. **261–262** (2013), 96–104. https://doi.org/10.1016/j.cma.2013.03.025.
- [19] V. Tu, F. Larsson, K. Runesson, and R. Jänicke, Deformation-dependent effective mobility in structural battery electrolytes, Int. J. Solids Struct. 315 (2025), 113342. https://doi.org/10.1016/j.ijsolstr.2025.113342.
- [20] V. Vajdova, P. Baud, and T.-f. Wong, Permeability evolution during localized deformation in Bentheim sandstone, J. Geophys. Res. 109 (2004), no. B10, B10406. https://doi.org/10.1029/2003JB002942.
- [21] S. Whitaker, Flow in porous media I: A theoretical derivation of Darcy's law, Transp. Porous Media 1 (1986), 3–25. https://doi.org/10.1007/BF01036523.
- [22] P. Wriggers, J. Korelc, and Ph. Junker, A third medium approach for contact using first and second order finite elements, Comput. Methods Appl. Mech. Eng. **436** (2025), 117740. https://doi.org/10.1016/j.cma.2025.117740.
- [23] G. Yang, S. Yu, J. Mo, Y. Li, Z. Kang, G. Bender, B. S. Pivovar, J. B. Green, D. A. Cullen, and F.-Y. Zhang, Impacts of catalyst nanolayers on water permeation and swelling of polymer electrolyte membranes, J. Power Sources 448 (2020), 227582. https://doi.org/10.1016/j .jpowsour.2019.227582.
- [24] A. A. Youssef, Q. Shao, and S. K. Matthäi, Computing relative permeability and capillary pressure of heterogeneous rocks using realistic boundary conditions, Transp. Porous Media 151 (2024), no. 8, 1729–1754. https://doi.org/10.1007/s11242-024-02092-x.

How to cite this article: D. R. Rollin, F. Larsson, K. Runesson, and R. Jänicke, *Deformation dependent permeability from variationally consistent homogenization*, GAMM-Mitteilungen. **48** (2025), e70010. https://doi.org/10.1002/gamm.70010

APPENDIX A. MATERIAL PARAMETERS FOR THE MATRIX PHASE

As example material, we consider an anode catalyst layer in a polymer electrolyte membrane water electrolyzer. The matrix material of this layer is assumed to be produced from Nafion® D2020 and Iridium particles. Since mechanical properties of this specific material have not been found in the literature, we use a rough estimation of elastic parameters. Firstly, we need parameters for the constituents of the matrix:

- We consider a Nafion® N117 membrane as reference material to find estimates for Nafion® D2020. For such a porous membrane a Young's modulus of $E_{\rm M}\approx 1.6$ GPa is assumed based on [10]. Estimating the porosity of the membrane to be $n_{\rm P}^{\rm M}\approx 0.5$ (cf, [8]), we choose $E_{\rm N}\approx \frac{E_{\rm M}}{n_{\rm P}^{\rm M}}=3.2$ GPa as Young's modulus of the pure Nafion®. Using a Poisson's ratio of $v_{\rm N}\approx 0.49$ as estimate for a polymer, we obtain the Lamé parameters $\lambda_{\rm N}\approx 52.6$ GPa and $G_{\rm N}\approx 1.07$ GPa.
- For Iridium, elastic parameters are taken from [12] to obtain the Lamé parameters $\lambda_{\rm I} \approx 228$ GPa and $G_{\rm I} \approx 210$ GPa.

Next, we need the volume fractions of the constituents. Assuming an Iridium content of $2 \cdot 10^3 \frac{\text{kg}}{\text{m}^3}$ (based on $2 \cdot \frac{\text{mg}}{\text{cm}^2}$ loading [13] and 10 μ m layer thickness [5]) and using the density of Iridium $\rho_{\text{I}} \approx 22.56 \cdot \frac{\text{kg}}{\text{m}^3}$ (cf. [3]), we estimate the

volume fraction of Iridium in the overall catalyst layer to be $n_{\rm I}^{\rm CL}\approx 0.089$. For an assumed porosity of about $n_{\rm P}^{\rm CL}\approx 0.5$ of the catalyst layer, the volume fraction of Nafion® is calculated as $n_{\rm N}^{\rm CL}\approx n_{\rm P}^{\rm CL}-n_{\rm I}^{\rm CL}=0.411$. The volume fractions of the two materials with respect to only the matrix phase are obtained as

$$n_{\rm I} = \frac{n_{\rm I}^{\rm CL}}{n_{\rm p}^{\rm CL}} = 0.178,$$
 (A1a)

$$n_{\rm N} = \frac{n_{\rm N}^{\rm CL}}{n_{\rm p}^{\rm CL}} = 0.822.$$
 (A1b)

Finally, we estimate the Lamé parameters for the matrix formed by Nafion® D2020 and Iridium particles as:

$$\lambda = n_{\rm N} \lambda_{\rm N} + n_{\rm I} \lambda_{\rm I} \approx 84 \text{ GPa},$$
 (A2a)

$$G = n_{\rm N}G_{\rm N} + n_{\rm I}G_{\rm I} \approx 38 \text{ GPa}. \tag{A2b}$$